Electron-energy-loss channels and plasmon confinement in supported silver particles

Rémi Lazzari,[1,*] Jacques Jupille,[1,†] and Jean-Marc Layet[2,‡]
[1]*Groupe de Physique des Solides, CNRS UMR 7588—Universités Paris 6 et 7, 2 Place Jussieu, 75251 Paris Cedex 05, France*
[2]*Université de Provence, Centre de Saint-Jérôme, UMR CNRS 6633, Equipe Plasma-Surface case 241, Avenue Escadrille Normandie-Niémen, 13397 Marseille Cedex 20, France*

(Received 13 December 2002; revised manuscript received 21 March 2003; published 31 July 2003)

The present paper is aimed at distinguishing the surface and particle contributions to the electron-energy-loss reflection spectrum from supported metallic particles in the thin layer limit $k_{\parallel}d^{*}\ll 1$, where $k_{\parallel}$ is the electron parallel momentum transfer and d^{*} the dielectric effective layer thickness. In the same way as with light excitation, the key constituents of the response of supported clusters are the cluster polarizabilities which create the long-range dipole oscillating field resulting in energy loss upon electron scattering. Contributions to the plasmon peak from either the substrate (Ag/Si, via the model) or a mixture of parallel and perpendicular excitations linked to the cluster shape (Ag/MgO, model and experiments) are identified. In the case Ag/MgO, a prototype for the study of plasmon excitation because of the negligible substrate contribution, a plasmon dispersion is observed even within a $k_{\parallel}$ range in which plasmon confinement is expected. This is interpreted as the signature of the island polarizabilities oscillatorlike behavior.

DOI: 10.1103/PhysRevB.68.045428 PACS number(s): 79.20.Uv, 73.22.Lp, 78.20.Bh

I. INTRODUCTION

Plasmon excitations in metals in either forms, surfaces,[1–7] thin layers,[8] embedded clusters,[9] and supported particles[10–12] have long attracted a tremendous scientific interest since these collective oscillations are a key tool for understanding the behavior of the electronic gas at surfaces and interfaces. Here, constant concern is the nonlocal dielectric response as a function of the dimension of the probed system, i.e., size of cluster or layer thickness, notably for silver (see for review, Ref. 7). The most often used means to experimentally probe the electronic structure of supported nanoparticles are photon excitation as surface differential reflectance (SDR) spectroscopy[10,13] or electron-energy-loss spectroscopy (EELS).[7] These two probes rely on the same physics for the coupling with the plasmon excitation through the electromagnetic field. Because of symmetry rule, the plasmon excitation of surfaces can not be probed directly with light reflection, but only with electrons, meanwhile for films or particles both techniques are relevant. They were much applied to the study of simple Drude metals such as alkali metals and to silver for understanding the screening role of *d* electrons in collective excitations. At high-momentum transfer, a ''blue shift'' is observed for silver particles on silicon.[12,14] In this case, a model for EELS cross section would permit the decoupling of the shape-support effect from the pure nonlocal behavior of the dielectric constant. In this respect, a clear link between the Mie optical excitation and the EELS response for islands on a surface is still missing.

However, the loss channels contributing to the EELS spectrum of supported clusters have not been identified yet. The present paper is aimed at clarifying the nature of the modes, their dependency on the substrate and the particle shape. The origin of the features observed in the loss spectrum of Ag/MgO is discussed as well as their dispersion with parallel momentum transfer through a modeling of the loss process. The model then allows a comparison between Ag/MgO and Ag/Si, MgO and silicon being chosen because of their different dielectric properties.

II. EXPERIMENTAL AND RESULTS

Experiments[15] have been carried out in an ultrahigh vacuum (UHV) chamber (base pressure of 3×10^{-8} Pa) equipped with a high-resolution electron-energy-losses spectrometer (HREELS LK2000) and a SDR setup. The substrate surface MgO(100) was produced by *ex situ* cleavage in air for HREELS experiments or in a glove bag in which dry nitrogen was circulating for the optical measurements. The glove bag was connected to the lock-load system of the UHV chamber such that the cleaved sample could be introduced in vacuum without any contact with the ambient air. The samples were cleaned by *in situ* heating at $T=1000$ K under oxygen partial pressure. Silver was evaporated from a Knudsen cell whose flux was calibrated by a quartz microbalance. An equivalent thickness of $e=0.15$ nm was deposited for the studied sample in HREELS and the thickness was continuously varied while recording the optical spectra in SDR. The SDR setup was already described elsewhere.[16,17] Briefly, it consists in recording the relative variation of the substrate reflectivity upon deposition of metal by illuminating the sample with UV-visible light (deuterium lamp) and by analyzing the reflected light with a spectrograph in either *p* or *s* polarization. The incident angle was imposed at $\theta_0=45°$ by the chamber feedthroughs. The electron-energy-loss system was run with an angle of incidence of $\theta_0=60°$ at an impact energy of $E=37$ eV. The energy resolution of the analyzer was set to $\delta E=35$ meV to allow for a reasonable counting rate. By varying the collection angle, the parallel wave vector was scanned with a resolution of $\delta k_{\parallel}=0.3$ nm^{-1}. During HREELS counting, substrate charging effects[18–20] were avoided by illuminating the sample with a defocused additional electron beam (1 keV-1 nA cm^{-2}).

The HREELS spectra for Ag/MgO are displayed in Fig. 1(a) as a function of the parallel momentum transfer which

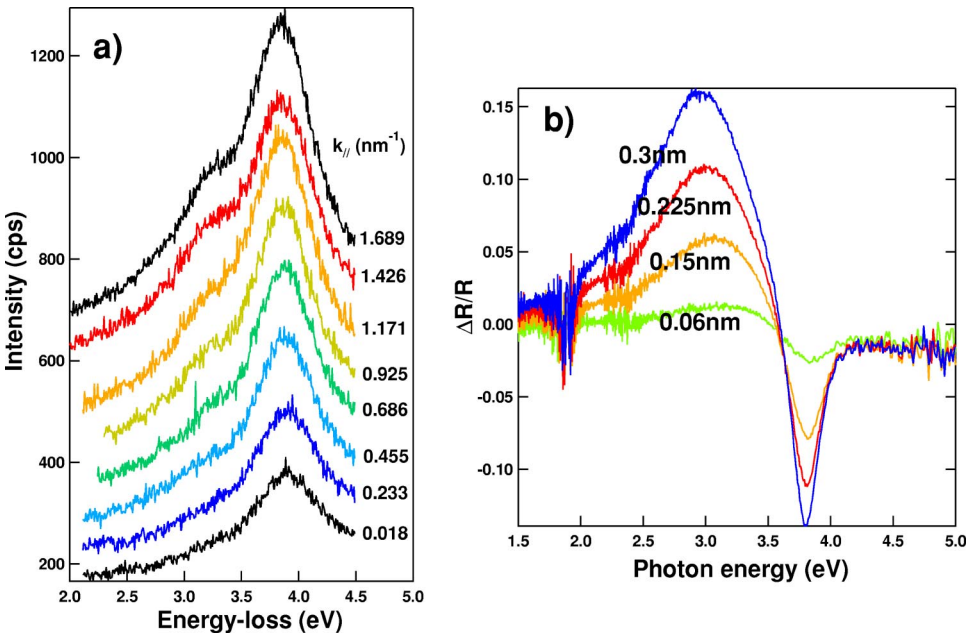

FIG. 1. (a) Experimental electron-energy-losses spectra for a Ag/MgO(100) cluster layer with an equivalent thickness of 0.15 nm. The spectra, shifted for a matter of clarity, were recorded at an impact energy of $E=37$ eV and an angle of incidence $\theta_0=60°$ for various parallel momentum transfers $k_\parallel$ [from Didier (Ref. 15), with permission]. (b) Experimental SDR spectra recorded (see text) in p polarization during vapor deposition of silver on a MgO(100) substrate at room temperature. The average silver thicknesses are given on each graph.

was calculated through momentum and energy conservation. The spectra present a peak with a shoulder at a frequency close to the surface plasmon mode for silver particles. As the substrate is nonabsorbing, these features can be safely assigned to such a mode. The puzzling fact in comparison to the already published HREELS curves for plasmon in clusters [Ag/C (Ref. 11)-Ag/Si (Refs. 8 and 12)] is the presence of a shoulder which develops and shifts with increasing parallel momentum transfer $k_\parallel$. These two components are analogous to the surface and interface plasmon of thin continuous film despite the fact that the silver overlayer on MgO is undoubtfully made, for such a coverage, of discontinuous particles.[16,21,22] The dispersion of these two features with $k_\parallel$, displayed in Fig. 2, was determined by a Lorentzian fit to the peak structure. Surprisingly, the nonzero slope of the dispersion points to a propagative behavior of the plasmon resonance whereas a confinement of the excitation is expected in the islands.[12] Moreover, an explanation based on the well-known quantum blue shift observed at high $k_\parallel$ value for silver surfaces[7,12,23] is not compatible with the opposite slopes versus $k_\parallel$ of the observed features.

Figure 1(b) shows the sequence of SDR spectra acquired during the silver deposition on MgO in p polarization. Two resonances of Mie type which appear around $E=3-3.8$ eV are ascribed to the excitations of the plasmon oscillations parallel and perpendicular to the substrate in the growing particles and have been previously modeled.[16,17,24–28] Drawing a parallel, at least for the energy positions, between the features observed by HREELS and the parallel and perpendicular plasmon resonances excited by the UV-visible light is tempting. However, it is not reconcilable with the observed dispersion with $k_\parallel$. A theoretical link between the two plasmon excitation mechanisms in supported metallic nanoparticles, i.e., photons and electrons, is thus needed to overcome this problem and to have a clear overview of the way in which the electron-energy-loss channels manifest themselves in the loss spectrum.

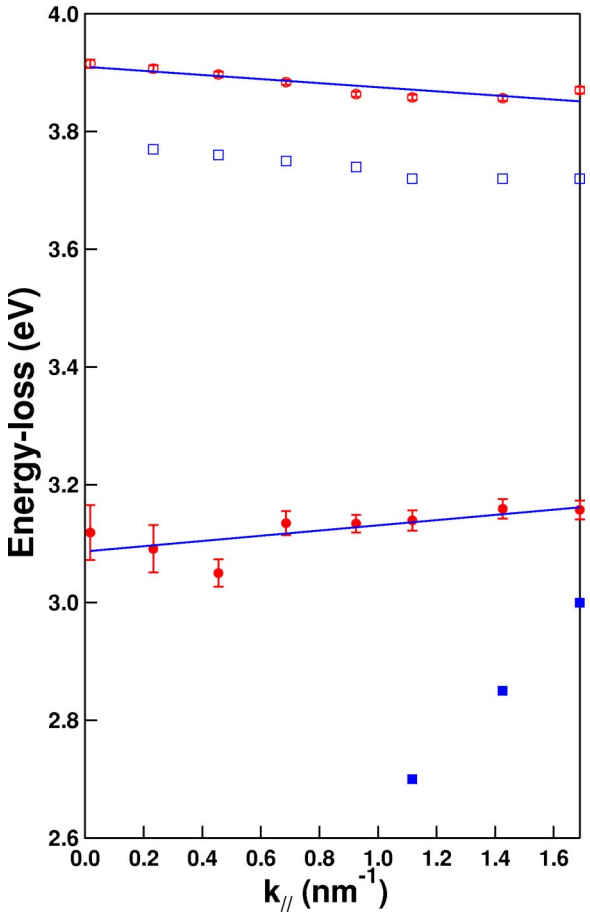

FIG. 2. Experimental dispersion (circles) of the two peaks of Fig. 1(a) as a function of $k_\parallel$. The straight lines correspond to a linear regression. The thin-plate dispersion curves, Eq. (4.2) (square), calculated with the bulk silver dielectric constant were added for comparison.

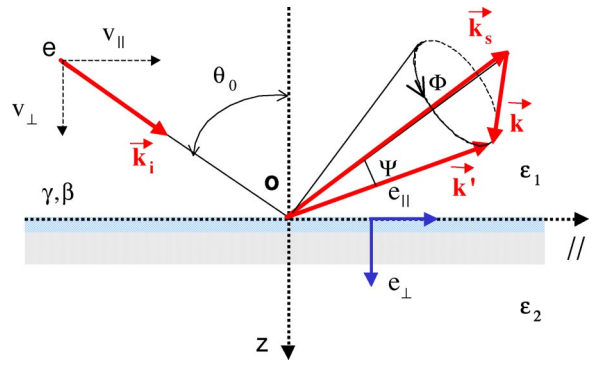

FIG. 3. The geometry for the calculation of electron-energy-losses cross section. An electron with velocity $(\mathbf{v}_\parallel, v_\perp)$ and wave vector $\mathbf{k}_i$ impinges on a surface of a substrate defined through its surface susceptibilities γ,β (see Sec. III A). It is scattered in the direction of $\mathbf{k}'$ around the specular direction $\mathbf{k}_s$.

III. COMPONENTS OF THE ELECTRON-ENERGY-LOSS SPECTRUM OF SUPPORTED CLUSTERS

In this section, the cross section for electron-energy losses is derived for a perturbed surface layer whose dielectric thickness d^* is much smaller than the depth probed by the electron $1/k_\parallel$, with $k_\parallel$ the parallel momentum transfer of the impinging electrons. A monoenergetic beam of electrons of charge e, mass m, energy E (a few tens of eV), wave vector $\mathbf{k}_i$, and velocity $\mathbf{v}=(v_\parallel, v_\perp)$ impinges with an incident angle θ_0 (Fig. 3). The origin of time $t=0$ is chosen to correspond to the electron reaching the surface at the origin O of the Cartesian frame with its z axis pointing downwards. Low-energy electrons penetrate very little into the solid. They are mainly scattered by the long-range Coulomb interaction which induces dielectric losses in the sample linked to the moving image charge. The energy losses being small with respect to the incident energy $(\hbar\omega \ll E)$, the electron velocity v is assumed not to be perturbed. The scattering direction of interest $\mathbf{k}'$ is close to the specular reflected beam $\mathbf{k}_s$ $(\psi,\phi \ll 1$, see Fig. 3). As v is much smaller than the speed of light, this phenomenon is described in the nonretarded approximation by the two Maxwell equations

$$\nabla\cdot\mathbf{D}=e\,\delta(\mathbf{r}-\mathbf{v}t), \tag{3.1a}$$

$$\nabla\times\mathbf{E}=\mathbf{0}, \tag{3.1b}$$

where $\mathbf{E},\mathbf{D}$ are the electric and displacement fields, respectively. $\mathbf{E}$ being derived from a potential $\mathbf{E}=-\nabla\Psi(\mathbf{r})$ [Eq. (3.1b)], the Poisson equation can be solved by introducing the dielectric constant of the various media $\epsilon_{(1,2)}$ and by using the Fourier transform in space and time, i.e., an expansion of the potential and fields of type $f(\mathbf{r},t)$ in surface waves:

$$f(\mathbf{k}_\parallel,z,\omega)=\int dt\int d^2r_\parallel \exp[i(\mathbf{k}_\parallel\cdot\mathbf{r}-\omega t)]f(\mathbf{r}_\parallel,z,t). \tag{3.2}$$

The final and classical result (see, for instance, Ref. 29) is

$$\Psi^{(1)}(\mathbf{k}_\parallel,z,\omega)=A_1\exp(k_\parallel z)-\Delta_0\left[\exp(k_\parallel z)-2\cos\left(\frac{z}{|v_\perp|}(\mathbf{k}_\parallel\cdot\mathbf{v}_\parallel-\omega)\right)\right], \quad z<0, \tag{3.3a}$$

$$\Psi^{(2)}(\mathbf{k}_\parallel,z,\omega)=B_2\exp(-k_\parallel z)+\Delta_0\exp(-k_\parallel z), \quad z>0, \tag{3.3b}$$

$$\text{with} \quad \Delta_0=\frac{1}{\epsilon_1\epsilon_0}\frac{e|v_\perp|}{k_\parallel^2 v_\perp^2+(\mathbf{k}_\parallel\cdot\mathbf{v}_\parallel-\omega)^2}. \tag{3.3c}$$

A_1, B_2 are two unknowns. These equations imply that the typical probed depth by the Coulomb field is proportional to $1/k_\parallel$. The frequency dependent dielectric constant is defined by $\epsilon(\omega,z)=\epsilon_1(\omega)\Theta(-z)+\epsilon_2(\omega)\Theta(z)$, with $\Theta(z)$ the step function. The substrate is supposed to be nonspatially dispersive and fully characterized by its dielectric constant $\epsilon_2(\omega)$.

The goal is now to identify the different energy-electron-loss channels which are involved in the differential scattering cross section. To go ahead, the above unknown parameters A_1, B_2 which appear in the expression of the potential, will be first determinated, within the framework of the excess field theory, as a function of surface susceptibilities linked to the particle polarizabilities parallel and perpendicular to the substrate.[30–34] They will be then used to compute the electric fields and to determine the loss function, prior to being applied to experimental findings.

A. The boundary conditions and the surface susceptibilities

Well known in the case of flat substrates or thin continuous films,[29,35,36] boundary conditions are far more complex on rough surfaces. The formalism developed by Bedeaux and Vlieger[30–34] to treat the optical properties of surfaces assumes that the perturbed surface layer thickness is much smaller than the wavelength of the incident wave. It is based on the concept of excess fields[32] in the Maxwell equations which stem from the difference between the real fields and the extrapolated bulk fields to the surface. For instance, the electric excess field is written as

$$\mathbf{E}(\mathbf{r},t)=\mathbf{E}_1(\mathbf{r},t)\Theta(-z)+\mathbf{E}_2(\mathbf{r},t)\Theta(z)+\mathbf{E}_{exc}(\mathbf{r},t), \tag{3.4}$$

where $\Theta(z)$ is the step function and $\mathbf{E}_1(\mathbf{r},t)$ and $\mathbf{E}_2(\mathbf{r},t)$ are the bulk fields extrapolated to the surface. Once introduced in the Maxwell equations, the excess field definitions give the following boundaries conditions for nonmagnetic media and in a stationary case:

$$\mathbf{E}_{2,\parallel}(\mathbf{r}_\parallel,z=0,\omega)-\mathbf{E}_{1,\parallel}(\mathbf{r}_\parallel,z=0,\omega)=\nabla_\parallel\mathcal{E}_{S,z}(\mathbf{r}_\parallel,\omega), \tag{3.5a}$$

$$D_{2,z}(\mathbf{r}_\parallel,z=0,\omega)-D_{1,z}(\mathbf{r}_\parallel,z=0,\omega)=-\nabla_\parallel\cdot\mathcal{D}_{S,\parallel}(\mathbf{r}_\parallel,\omega), \tag{3.5b}$$

where $\boldsymbol{\nabla}_{\parallel}$ designates the two-dimensional gradient operator $\boldsymbol{\nabla}_{\parallel}=(\partial/\partial x,\partial/\partial y)$. The excess fields integrated perpendicularly to the surface previously introduced are defined through

$$\boldsymbol{\mathcal{E}}_S(\mathbf{r}_{\parallel},\omega)=\int_{-\infty}^{+\infty}dz\mathbf{E}_{exc}(\mathbf{r}_{\parallel},z,\omega)$$

and

$$\boldsymbol{\mathcal{D}}_S(\mathbf{r}_{\parallel},\omega)=\int_{-\infty}^{+\infty}dz\mathbf{D}_{exc}(\mathbf{r}_{\parallel},z,\omega). \tag{3.6}$$

The above relations can be obtained in an analogous way by gathering the contributions of excess fields in a singular term at the surface of the substrate[30,31] and by imposing that $\mathcal{D}_{S,z}(\mathbf{r}_{\parallel},\omega)=\mathcal{E}_{S,\parallel}(\mathbf{r}_{\parallel},\omega)=0$:

$$\mathbf{E}(\mathbf{r}_{\parallel},z,\omega)=\mathbf{E}_1(\mathbf{r}_{\parallel},z,\omega)\Theta(-z)+\boldsymbol{\mathcal{E}}_S(\mathbf{r}_{\parallel},\omega)\delta(z)+\mathbf{E}_2(\mathbf{r}_{\parallel},z,\omega)\Theta(z), \tag{3.7a}$$

$$\mathbf{D}(\mathbf{r}_{\parallel},z,\omega)=\mathbf{D}_1(\mathbf{r}_{\parallel},z,\omega)\Theta(-z)+\boldsymbol{\mathcal{D}}_S(\mathbf{r}_{\parallel},\omega)\delta(z)+\mathbf{D}_2(\mathbf{r}_{\parallel},z,\omega)\Theta(z). \tag{3.7b}$$

The so-called surface susceptibilities γ and β make the link between the integrated excess fields and the value of the bulk fields at $z=0$. For a homogeneous and isotropic interface, these relations are

$$\boldsymbol{\mathcal{D}}_{S,\parallel}(\mathbf{r}_{\parallel})=\epsilon_0\frac{\gamma(\omega)}{2}[\mathbf{E}_{1,\parallel}(\mathbf{r}_{\parallel},z=0)+\mathbf{E}_{2,\parallel}(\mathbf{r}_{\parallel},z=0)], \tag{3.8a}$$

$$\mathcal{E}_{S,z}(\mathbf{r}_{\parallel})=-\frac{\beta(\omega)}{2\epsilon_0}[D_{1,z}(\mathbf{r}_{\parallel},z=0)+D_{2,z}(\mathbf{r}_{\parallel},z=0)]. \tag{3.8b}$$

In the case of clusters on a surface, the surface susceptibilities γ,β are linked to the cluster polarizabilities $\alpha_{\parallel},\alpha_{\perp}$ parallel and perpendicular to the substrate: $\gamma=\rho\alpha_{\parallel}/\epsilon_0$ and $\beta=\rho\alpha_{\perp}/(\epsilon_1^2\epsilon_0)$ (ρ the number of particles per unit of surface). These have been determined in great detail, in the quasistatic limit, for supported clusters[17,24,26–28,30,37] through a multipolar expansion of the potential. Expressions γ,β were also derived for rough surfaces.[30,38] To apply the surface susceptibilities formalism to electron-energy-losses by gathering all the excess fields in a singular term at the surface, the surface layer should not perturb significantly the Coulomb field. This implies that the probed depth is much higher than the surface "dielectric thickness" d^*: $k_{\parallel}d^*\sim k_{\parallel}\gamma\sim k_{\parallel}\beta\ll 1$. It is worth noting that the nonretarded interaction approximation used in Eqs. (3.1), $\omega/c\ll k_{\parallel}$, and the working limit $k_{\parallel}d^*\ll 1$ are easily fulfilled for thin films. For example, typical values of energy loss $\hbar\omega=2.5$ eV, layer thickness $d^*=0.15$ nm, and parallel momentum transfer $k_{\parallel}=0.2$ nm^{-1} lead to $k_{\parallel}=16\omega/c$ and $k_{\parallel}d^*=0.03$.

Using $\mathbf{E}(\mathbf{r})=-\boldsymbol{\nabla}\Psi(\mathbf{r})$ and Eqs. (3.3) and (3.5)–(3.8), the unknowns A_1,B_2 are found to fulfill a linear system of equations whose coefficients are weighted by the surface susceptibilities:

$$A_1\left[1-\frac{\epsilon_1}{2}k_{\parallel}\beta\right]+B_2\left[-1+\frac{\epsilon_2}{2}k_{\parallel}\beta\right]=-\frac{\epsilon_1+\epsilon_2}{2}\Delta_0 k_{\parallel}\beta,$$

$$A_1\left[\epsilon_1+\frac{1}{2}k_{\parallel}\gamma\right]+B_2\left[\epsilon_2+\frac{1}{2}k_{\parallel}\gamma\right]=\Delta_0(\epsilon_1-\epsilon_2-k_{\parallel}\gamma). \tag{3.9}$$

A discussion on the determinant of this system is given in the Appendix in terms of surface modes. Solving the system Eq. (3.9) to first order in $k_{\parallel}\gamma$ and $k_{\parallel}\beta$ leads to

$$A_1=-\Delta_0\frac{\epsilon_2-\epsilon_1}{\epsilon_2+\epsilon_1}\left[1+\frac{2\epsilon_1 k_{\parallel}}{\epsilon_2^2-\epsilon_1^2}(\gamma+\beta\epsilon_2^2)\right], \tag{3.10a}$$

$$B_2=-\Delta_0\frac{\epsilon_2-\epsilon_1}{\epsilon_2+\epsilon_1}\left[1+\frac{2\epsilon_1 k_{\parallel}}{\epsilon_2^2-\epsilon_1^2}(\gamma-\beta\epsilon_1\epsilon_2)\right]. \tag{3.10b}$$

If $\gamma=\beta=0$, one recovers the classical image term $A_1=B_2=-\Delta_0(\epsilon_2-\epsilon_1)/(\epsilon_2+\epsilon_1)$.[39,40]

B. The differential scattering cross section for electron-energy losses

To derive the scattering cross section, the relevant quantity is the integrated electron-energy-losses which comes from the induced dielectric losses in the substrate and in the surface layer:

$$W=\mathrm{Re}\left[\int dt\int d^3r\mathbf{E}(\mathbf{r},t)\cdot\frac{\partial}{\partial t}\mathbf{D}(\mathbf{r},t)\right]. \tag{3.11}$$

Of course, in the dielectric approach, the electron-impact contribution is neglected.[29] Using the decomposition of the field in plane waves parallel to the surface, one ends up with

$$W=\frac{1}{(2\pi)^3}\mathrm{Im}\left[\int dz\int d\omega\int d^2k_{\parallel}\omega\mathbf{E}(\mathbf{k}_{\parallel},\omega,z)\cdot\mathbf{D}^*(\mathbf{k}_{\parallel},\omega,z)\right]$$
$$=\int d^2k_{\parallel}\int d(\hbar\omega)\hbar\omega\mathcal{P}(\hbar\omega,k_{\parallel}), \tag{3.12}$$

with $\mathbf{D}^*$ the complex conjugate of the displacement field. In the above relation, $\mathcal{P}(\hbar\omega,k_{\parallel})$ is the scattering probability of an electron with a energy loss $\hbar\omega$ and a momentum transfer $k_{\parallel}$.

To go ahead, all the fields in Eqs. (3.7) have to be expressed using the definitions of the potential in media 1,2 [Eq. (3.3)], that of the surface susceptibilities [Eqs. (3.8)] and the expressions [Eqs. (3.10)]. In particular, the singular term at $z=0$ [Eqs. (3.7)] is given in terms of the integrated excess fields

$$\mathcal{D}_{S,\parallel}(\mathbf{k}_\parallel,\omega) = -\frac{2i\epsilon_1\epsilon_0\Delta_0\mathbf{k}_\parallel\gamma}{(\epsilon_1+\epsilon_2)^2}\left[\epsilon_1+\epsilon_2-k_\parallel\gamma-\frac{\epsilon_2}{2}(\epsilon_2-\epsilon_1)k_\parallel\beta\right], \tag{3.13a}$$

$$\mathcal{E}_{S,z}(\mathbf{k}_\parallel,\omega) = -\frac{2i\epsilon_1\Delta_0 k_\parallel\beta}{(\epsilon_1+\epsilon_2)^2}\left[\epsilon_2(\epsilon_1+\epsilon_2)-\frac{\epsilon_1-\epsilon_2}{2}k_\parallel\gamma-\epsilon_1\epsilon_2^2 k_\parallel\beta\right]. \tag{3.13b}$$

As $\Theta(\pm z)\,\delta(z)=\frac{1}{2}\delta(z)$, the scalar product in Eq. (3.12) takes the following form:

$$\mathbf{E}.\mathbf{D}^* = \underbrace{\mathbf{E}_1.\mathbf{D}_1^*\Theta(-z)}_{(1)} + \underbrace{\mathbf{E}_2.\mathbf{D}_2^*\Theta(z)}_{(2)} + \underbrace{\frac{1}{2}\boldsymbol{\mathcal{E}}_S.[\mathbf{D}_1^*+\mathbf{D}_2^*]\delta(z)}_{(3)} + \underbrace{\frac{1}{2}\boldsymbol{\mathcal{D}}_S^*.[\mathbf{E}_1+\mathbf{E}_2]\delta(z)}_{(4)} + \underbrace{\boldsymbol{\mathcal{E}}_S.\boldsymbol{\mathcal{D}}_S^*\,\delta(z)}_{(5)}. \tag{3.14}$$

Term (1), i.e., $\mathbf{E}_1.\mathbf{D}_1^*=\epsilon_1\epsilon_0|\mathbf{E}_1|^2$ does not contribute to the energy losses because ϵ_1 must be real (vacuum in practical case) to allow for an undisturbed propagation of the electron. Term (5) equals zero since the excess fields $\boldsymbol{\mathcal{E}}_S$ and $\boldsymbol{\mathcal{D}}_S^*$ are orthogonal. After integration over z in Eq. (3.12), and using Eqs. (3.3) and (3.13) the remaining terms (2)–(4) can be calculated to first order in $k_\parallel\gamma$, $k_\parallel\beta$ and inserted in Eq. (3.12) to give

$$\mathcal{P}(\hbar\omega,k_\parallel) = \frac{\epsilon_1^2\epsilon_0\Delta_0^2 k_\parallel}{2\pi^3\hbar^2}\left\{\mathrm{Im}\left[\frac{-1}{\epsilon_1+\epsilon_2}\right]\left[1-k_\parallel\mathrm{Re}\left(\frac{\gamma-\beta\epsilon_1\epsilon_2}{\epsilon_1+\epsilon_2}\right)\right] + k_\parallel\mathrm{Im}[\beta]\left|\frac{\epsilon_2}{\epsilon_1+\epsilon_2}\right|^2 + k_\parallel\mathrm{Im}[\gamma]\left|\frac{1}{\epsilon_1+\epsilon_2}\right|^2\right\}. \tag{3.15}$$

However, one has to keep in mind that Eq. (3.15) is restricted only to small momentum transfer $k_\parallel$. Since experimentally the electrons are discriminated in energy in an out-specular direction given by $\mathbf{k}'$ in a solid angle $d\Omega$, the elementary volume in $k_\parallel$ space can be expressed as a function of $d\Omega$ (Refs. 29 and 35) for low-energy losses $\hbar\omega\ll E$ and close to the specular beam $\psi,\phi\ll 1$:

$$d^2k_\parallel = \frac{m^2v_\perp^2}{\hbar^2\cos\theta_0}d\Omega. \tag{3.16}$$

Finally, the differential cross section for electron-energy-losses is

$$\frac{d^2\mathcal{S}}{d(\hbar\omega)d\Omega} = \frac{m^2e^2}{2\pi^3\hbar^4\epsilon_0\cos\theta_0}\frac{k_\parallel v_\perp^4}{[k_\parallel^2v_\perp^2+(\mathbf{k}_\parallel\cdot\mathbf{v}_\parallel-\omega)^2]^2} \times\left\{\mathrm{Im}\left[\frac{-1}{\epsilon_1+\epsilon_2}\right]\left[1-k_\parallel\mathrm{Re}\left(\frac{\gamma-\beta\epsilon_1\epsilon_2}{\epsilon_1+\epsilon_2}\right)\right] + k_\parallel\mathrm{Im}[\beta]\left|\frac{\epsilon_2}{\epsilon_1+\epsilon_2}\right|^2 + k_\parallel\mathrm{Im}[\gamma]\left|\frac{1}{\epsilon_1+\epsilon_2}\right|^2\right\}. \tag{3.17}$$

This equation allows one to compute EELS spectra in the limit $k_\parallel d^*\ll 1$ for any surface layer morphology, provided there is the knowledge of the surface susceptibilities.

Three important terms appear in Eq. (3.17). The kinematical prefactor, which contains the geometrical constraints for the scattering shows that loss intensity peaks when the velocity of the electron matches the surface wave phase $\mathbf{k}_\parallel\cdot\mathbf{v}_\parallel=\omega$; this is the well-known ''surf-riding'' condition of optimal coupling between the incident electron and the excited surface wave.[29,35,41] Usually, it leads to an $1/\omega^4$ dependence in energy. The loss term is divided in two parts, weighed by the probed depth $1/k_\parallel$. The first one is the classical surface loss function in $\mathrm{Im}[-1/(\epsilon_1+\epsilon_2)]$ linked to the imaginary part of ϵ_2, thus to dissipative processes inside the substrate. Note that this factor is modified by a term in $k_\parallel\gamma,k_\parallel\beta$ which accounts for the screening of the field by the overlayer and for the modified image term inside the substrate. The other factors

$$\mathrm{Im}[\beta]\left|\frac{\epsilon_2}{\epsilon_1+\epsilon_2}\right|^2+\mathrm{Im}[\gamma]\left|\frac{1}{\epsilon_1+\epsilon_2}\right|^2 \tag{3.18}$$

describe the absorption of energy inside the surface layer. The terms in γ and β are weighted according to the classical ''dipole rule.'' It is clear that, for a substrate with strong dielectric constant, the parallel excitation is ''canceled'' by the image term inside the substrate. This approach is equivalent to the thin-plate model[29] with the advantage that the dielectric constant ϵ_c and the thickness d^* of the plate do not appear explicitly. In this special case,

$$\gamma=d(\epsilon_c-\epsilon_1),\quad \beta=d\left(\frac{1}{\epsilon_1}-\frac{1}{\epsilon_c}\right). \tag{3.19}$$

C. Comparison between cross sections for optical and electron probes

Another common way to probe the dielectric properties of surface is the use of surface sensitive optical techniques such as SDR. In both cases, optics and electron-energy-loss spectroscopy, the inelastic processes are due to the same physical phenomenon, the surface vibrating dipole. The electric field of the incident light polarizes the surface entities (molecules, metallic islands, roughness, and so on), leading to a possible dissipative channel and to optical absorptions. For an electron, because of its movement, the generated Coulomb field contains all kind of wave vectors and frequencies allowing

coupling with any surface vibration, in particular, when the phase-matching conditions [see Eq. (3.17) and remark below] are met.

In the framework of the surface susceptibilities model,[30,31] the change in reflectivity in comparison to bare nonabsorbing substrate in p,s polarization at incident angle θ_0 is given by

$$\frac{\Delta R_s}{R_s} = 4\frac{\omega}{c}\frac{\sqrt{\epsilon_1}\cos\theta_0}{\epsilon_2-\epsilon_1}\mathrm{Im}(\gamma), \tag{3.20a}$$

$$\frac{\Delta R_p}{R_p} = 4\frac{\omega}{c}\frac{\sqrt{\epsilon_1}\cos\theta_0}{(\epsilon_2-\epsilon_1)(\epsilon_2\cos^2\theta_0-\epsilon_1\sin^2\theta_0)} \times[(\epsilon_2-\epsilon_1\sin^2\theta_0)\mathrm{Im}(\gamma)-\epsilon_2^2\epsilon_1\sin^2\theta_0\mathrm{Im}(\beta)]. \tag{3.20b}$$

Equations (3.20) show clearly that in p polarization, two components of the electric field can probe both parallel and perpendicular excitations, whereas in s polarization the electric field is only parallel to the surface. Equivalent to the thin-plate model,[42] these equations obey to the "dipole selection rule" with $1/\epsilon_2$ ratio between the parallel β and perpendicular γ terms. In the EELS cross section, Eq. (3.17), the parallel/perpendicular ratio does not depend on the angle of incidence of the electron beam, which only induces a global change in intensity. On the contrary, in optics, the strength of the two components of the excitating electric field depends on both the angle of incidence and the beam polarization.

IV. ELECTRON-ENERGY-LOSSES SPECTRA FOR ISLANDS LAYERS: THE CASES OF Ag/MgO AND Ag/Si

In the following, the above model is applied to the case of silver island films. The surface susceptibilities which come into play in Eq. (3.17) are linked to the island polarizabilities. The particles are approximated by truncated sphere or spheroids and their polarizabilities are computed by solving, in the quasistatic regime, the Laplace equation under an external applied field, using a previously described multipolar expansion of the potential.[17,24–28,30,37,43] The used bulk dielectric constants are tabulated values[44] (Fig. 4). For convenience, neither interparticle dipolar coupling nor finite-size effects in the dielectric constants have been accounted for in the polarizability calculations.

A. The particle shape

Already highlighted in previous works[17,24,26,27] in the case of the optical response, the shape of the island and, in particular, its aspect ratio $\mathcal{A}=2R_{app}/H$, defined as the island apparent diameter (as seen from above) divided by its height, influences strongly its dielectric response via the island polarizability. In Fig. 5, the simulated Ag/MgO EELS spectra [Eq. (3.17)] are shown for a truncated sphere. Upon increasing the aspect ratio of the particle, two peaks appear in the EELS cross section which are mainly linked to the plasmon modes inside the cluster. To the first approximation, the low-energy excitation is associated to the dipole parallel to the substrate and the high-energy one to the dipole normal to the surface. Between these, a mode of quadrupolar[25–27] nature develops. Note that for islands with a low aspect ratio (close to the spherical shape) with a high contact angle, as it is expected for a noble metal on a wide band-gap oxide,[45,46] the two resonances are mixed up in a unique broad peak (see below) centered below 3.5 eV (the surface-plasmon frequency of a silver sphere in vacuum) because of the red shift caused by the depolarization field induced by the substrate.[26]

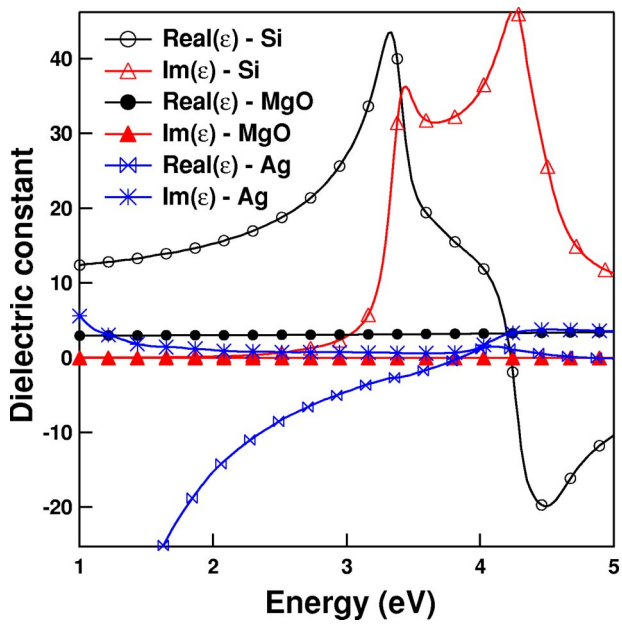

FIG. 4. Dielectric constant of Si, MgO, and Ag from Ref. 44. Notice the very flat MgO dielectric function in the range of interest.

B. Substrate-induced plasmon splitting and dissipation

As it is illustrated by comparing two substrates (MgO and Si) with different dielectric constants (see Fig. 4), the influence of the substrate on the dielectric response of a supported film is twofold.

First, the shape-induced plasmon splitting of the absorption modes[24,26,27,47] depends strongly on the dielectric constant. For a dipole parallel (perpendicular) to the surface, the depolarization field created by the image dipole reduces (increases) the restoring force acting on the electron cloud, thus inducing a softening (strengthening) of the vibration. This results in a red shift (blue shift) of the associated mode, as shown in Fig. 6 for supported silver hemispheroids with an aspect ratio of $\mathcal{A}=4$ covering 50% of the surface. Such a set of parameters is consistent with the growth of flat silver clusters on Si(111) (Refs. 14 and 48–50) which percolate at an average thickness of 4 ML (monolayer) at room temperature. If for MgO substrate [$\epsilon\simeq 3$, Fig. 6(c)] both parallel and perpendicular "dipolar" resonances are present in the plotted energy range, for Si [$\epsilon\simeq 10$, Fig. 6(b)], the parallel component is rejected far in the low-energy part of the spectrum (below 1.5 eV). The intermediate-energy peaks ($E=1.75$ eV) in the γ term are modes of quadrupolar order.[26,27] In addition, the contribution from the parallel po-

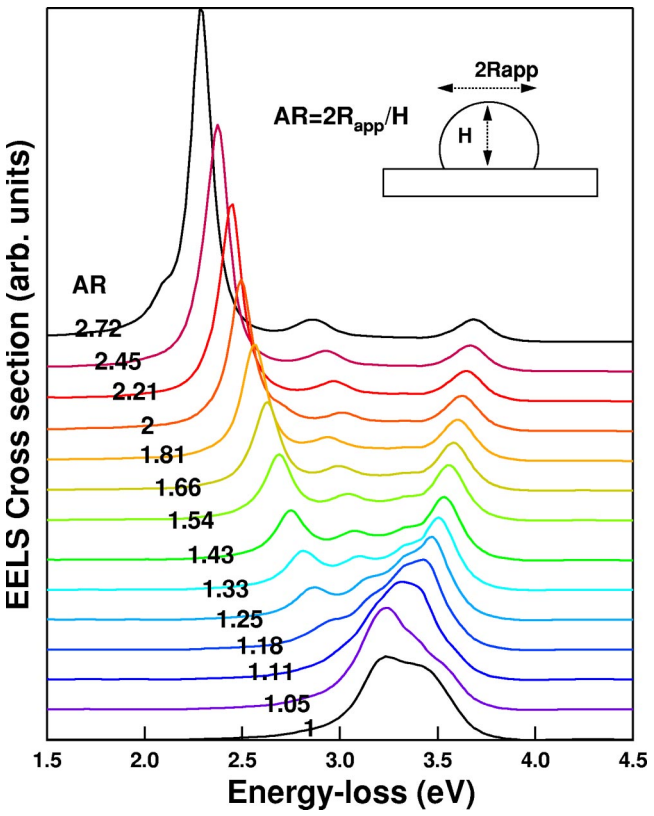

FIG. 5. Model spectra calculated for truncated spheres of silver supported on MgO to show the influence of the particle aspect ratio on the EELS cross section. Due to the poor wetting of MgO by silver, the real case is close to full sphere. The aspect ratio $\mathcal{A}$ is ranging from embedded sphere $\mathcal{A}=2.72$ to full sphere $\mathcal{A}=1$. The island polarizabilities have been computed up to multipolar order $M=32$ (Ref. 17). For the sake of clarity, the spectra have been shifted with respect of each other and normalized by the mean film thickness. The other parameters are $E=40$ eV, $k_{\parallel}=0.02$ nm^{-1}, and $\theta_0=60°$.

larizability γ tends to cancel for high values of the dielectric constant. This difference of dielectric behavior manifests itself in the polarization process of the island. Figure 7 displays the equipotential lines obtained by polarizing the island with a field either parallel (top panel) or perpendicular (bottom panel) to the surface at energies corresponding to the maxima of absorption. For MgO, the equipotential lines penetrate inside the substrate. The external field polarizes the island leading to a dipolelike behavior in both perpendicular and parallel directions. In a very different way, the silicon substrate and the supported cluster both behave as equipotential volumes (metal-like behavior) which repel the electric fields when applied perpendicular to the surface.

Second, a dissipative process is linked to the imaginary part of the dielectric constant. For silicon, the onset of interband transitions[51] is close to the plasmon excitation for silver. As electrons can induce indirect transition, at variance with optical probes, the surface excitation of the substrate is mixed with the overlayer absorption. To discriminate the two contributions, one has to vary the probed depth ($1/k_{\parallel}$), as highlighted in Fig. 6 for Si with (a) $k_{\parallel}=0.02$ nm^{-1} and (b) $k_{\parallel}=0.002$ nm^{-1}. Neglecting size-induced broadening, an important consequence is that the width of the resonance cannot be unambiguously connected to the lifetime of the plasmon oscillation. On the contrary, in the probed spectral range, the absorption within a wide band-gap compound such as MgO is negligibly small. In Fig. 6(c), the computed plateau after 4 eV is simply a signature of the *d-sp* interband transitions in silver. The system Ag/MgO appears as an archetype of plasmon confinement in nanometric islands, without any interference with substrate absorption.

C. Experimental high-resolution energy losses and optical spectra for Ag/MgO

Following the above discussion, the two features seen in the Ag/MgO(100) EELS spectrum can be interpreted as sig-

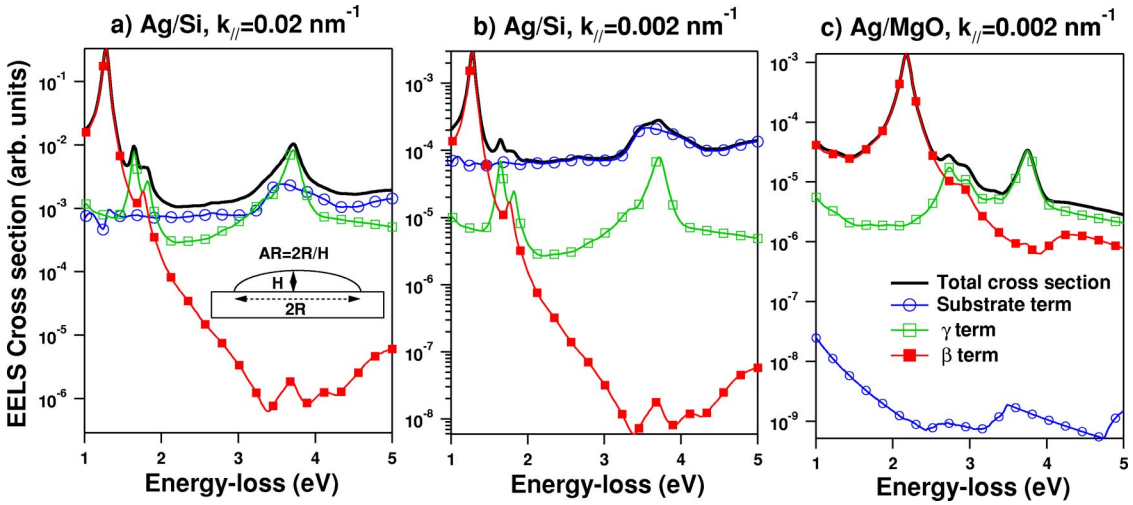

FIG. 6. Calculated EELS cross section for supported silver hemispheroidal particle with a radius of $R=5$ nm and an aspect ratio of $\mathcal{A}=4$ covering 50% of the substrate (equivalent thickness 0.8 nm—multipolar order $M=32$). The substrate nature and the parallel momentum transfer are indicated above figures. The various components of the cross sections have been detailed [see Eq. (3.17)]. The $E=40$ eV electron beam impinges under the surface at $\theta_0=60°$ incident angle.

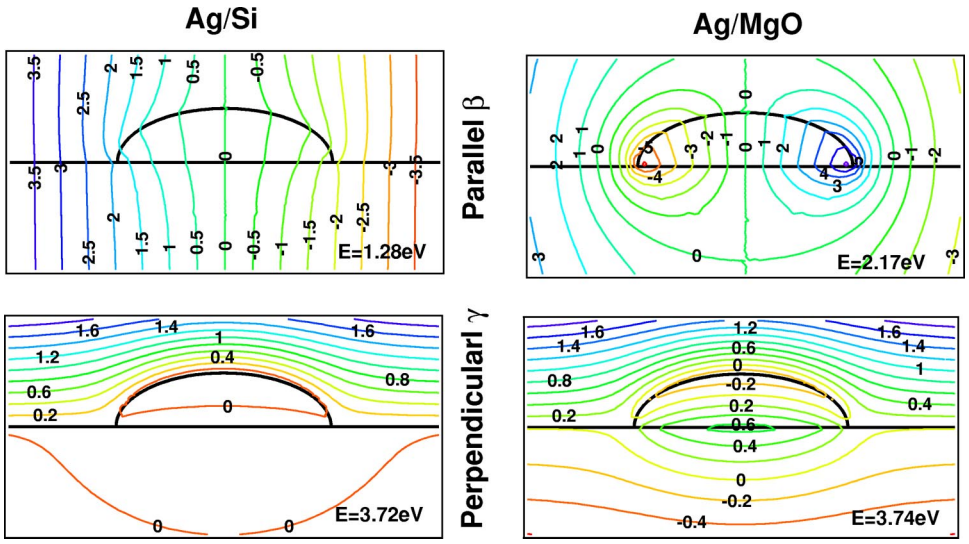

FIG. 7. Equipotential lines in normalized unit of E_0R for silver cluster on Si or MgO polarized by an applied field E_0 either parallel (top panels) or perpendicular (bottom panels) to the surface at energies of the extrema of Im(β) and Im(γ) (see Fig. 6).

natures of the two components of the surface susceptibilities, parallel γ and perpendicular β to the substrate. Indeed, these components were not simultaneously seen in the case of a silicon substrate[12] because the high particle aspect ratio and the coupling with the substrate result in a shift of the parallel resonance towards low energy. In Ref. 8, such a double-peak structure was observed around $E=1.5$ eV for Ag/Si and interpreted as the surface-interface plasmon of a thin continuous film. For Ag/C,[11] the change in shape of the spectra with $k_\parallel$ is likely due to the same effect of spherical shape as in the case of Ag/MgO.

Such an assignment is confirmed by the experimental SDR spectra [Fig. 1(b)] which shows the same type of structures at $E=3.1$ eV and $E=3.8$ eV. An attempt to adjust the SDR spectrum with a reasonable layer morphology is given in Fig. 8. The parameters obtained for truncated sphere $R=1.2$ nm, $\mathcal{A}=1.43$, and $\rho=3.5\times10^{12}$ cm^{-2} are in agreement with Refs. 21 and 22 and give the right equivalent thickness. Computed particle polarizabilities were renormalized by the interparticle dipolar interactions.[30,33,34] Because of the low size of the clusters, some classical finite-size corrections[9,52] were applied to the dielectric constant of silver:

$$\epsilon_m(\omega)=\epsilon_B(\omega)+\frac{\omega_p^2}{\omega^2+i\omega\tau_B^{-1}}-\frac{\omega_p^2}{\omega^2+\Sigma(R)+i\omega\tau(R)^{-1}}, \tag{4.1}$$

with $\omega_p=9.17$ eV the plasmon frequency of the s electrons only, $\hbar/\tau_B=0.018$ eV the bulk relaxation time, and $\epsilon_B(\omega)$ the bulk dielectric constant. Such corrections introduced through $\tau(R)$ and $\Sigma(R)$ affect only the s electrons which participate in the collective plasmon oscillation. They involve (i) a correction of the relaxation time link to the scattering of the electrons at the surface $\hbar/\tau(R)=\hbar/\tau_B+\hbar v_F/R$ ($v_F=0.91$ eV nm, the Fermi velocity) and (ii) a quantum blue shift linked to the spillout of the s electrons at the surface which reduces the coupling between s and the localized d electrons of silver;[52] $\Sigma(R)=-1.126S/V$ eV^2 nm^{-1} is taken proportional to the surface S over volume

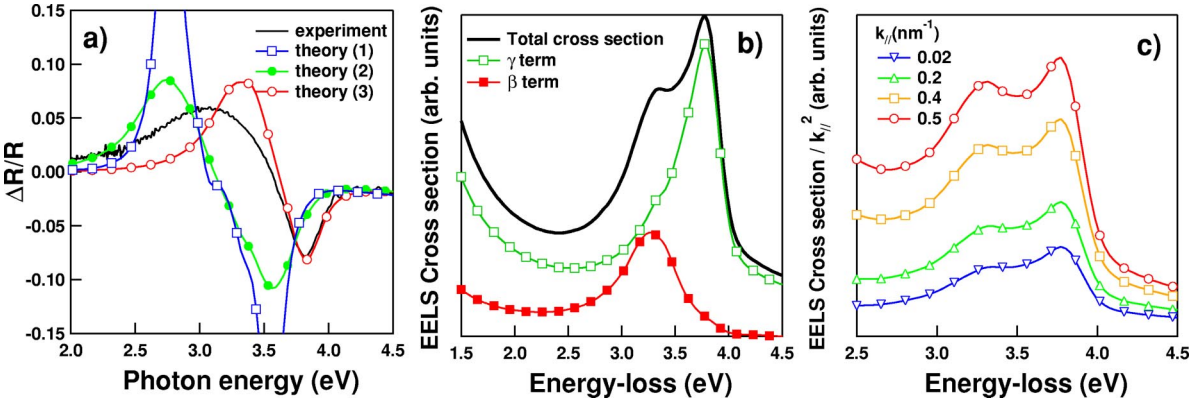

FIG. 8. (a) Experimental and theoretical simulated SDR spectra for an island layer of 0.15 nm taken at a $\theta_0=45°$ incident angle. The layer morphology is described by truncated spheres with $R=1.2$ nm, $\mathcal{A}=1.43$ at a density of $\rho=3.5\times10^{12}$ cm^{-2}. In theory 1, the silver bulk dielectric constant is used. In theory 2, a finite-size correction is applied to the plasmon lifetime, whereas in theory 3, in addition, a blue shift proportional to the surface/volume ratio is also added. (b) Simulated EELS spectra with the same parameters as in theory 3 with the two components parallel β and perpendicular γ ($E=37$ eV, $k_\parallel=0.02$ nm^{-1}, $\theta_0=60°$). (c) Calculated EELS spectra versus the parallel momentum transfer $k_\parallel$. The spectra have been rescaled by $k_\parallel^2$ [see Eq. (3.17)]. Otherwise, same parameters as in (b).

V ratio as suggested by previous experimental and theoretical works.[12,52] Spectra intensity and shape are reasonably accounted for in Fig. 8. The remaining discrepancy between the calculated (3.1 eV) and the experimental (3.3 eV) energy of the low-energy peak could come from the size and shape distribution and from finite-size corrections. Despite this fact, the order of magnitude of the signal and the spectral shape are well reproduced within a reasonable layer morphology. It is worth noting on simulated spectra of Fig. 8(a) (curves theory 2 and theory 3) that the surface/volume effect $\Sigma(R)$ induces very different energy shifts for the surface susceptibilities and thus for the SDR resonances, compared to the bulk silver dielectric constant.

With the same morphological parameters, the computed EELS spectrum of Fig. 8(b) for $k_{\parallel}=0.02$ nm^{-1} agrees well with experiment. The enhancement with $k_{\parallel}$ of the shoulder on the low-energy side of the main feature [Fig. 8(c)] can be partially related to the kinematical prefactor of ''surf riding'' [Eq. (3.17)]. As a result of the $1/\omega^4$ dependence, the relative intensity of the low-energy side of the loss spectrum is increasing with $k_{\parallel}$.

D. Dispersion of electron-energy-losses for Ag/MgO

Further insight can be gained by studying the dispersion of the two structures with parallel momentum transfer. These curves displayed in Fig. 2 have been obtained by fitting the data with two Lorentzian peaks, as suggested by the spectral representation of the cluster polarizabilities.[26,27,53] As a matter of comparison, the dispersion relations given by the pole of the loss function for a thin continuous layer[29] are displayed in Fig. 2:

$$\frac{d^2\mathcal{S}}{d\hbar\omega d\Omega}\sim \mathrm{Im}\left(\frac{-1}{\xi(k_{\parallel},\omega,d)+1}\right)$$

with

$$\xi(k_{\parallel},\omega,d)=\epsilon_m(\omega)\frac{\epsilon_m(\omega)\tanh(k_{\parallel}d)+\epsilon_2}{\epsilon_2\tanh(k_{\parallel}d)+\epsilon_m(\omega)}. \qquad (4.2)$$

$\epsilon_m(\omega)$ stands for the dielectric constant of the layer of thickness *d*. The agreement with such a continuous layer model (which was, in some respect, already observed in Ref. 8) is rather poor since the discontinuous nature of the layer is ignored. Instead, the generalized dispersion relations for surface waves [Eqs. (A1)–(A4)] should be used. By considering that the islands are polarizable entities with a small damping, the theory leads to two linear branches of dispersion with opposite signs, as observed experimentally in Fig. 2. A linear regression gives the cluster plasmon frequencies $\omega_{\parallel}=3.08\pm0.02$ eV and $\omega_{\perp}=3.91\pm0.01$ eV, and the ''dielectric effective thicknesses'' $d_{\parallel}^{*}=0.071\pm0.02$ nm and $d_{\perp}^{*}=0.012\pm0.001$ nm. As expected, the eigenfrequencies of the island polarizabilities are blue shifted in comparison to that of a silver sphere, mainly because of the surface over volume term $\Sigma(R)$. The ratio R_0 of the parallel and perpendicular oscillator strengths is equal to $R_0=F_{\parallel}/F_{\perp}=d_{\parallel}^{*}\omega_{\parallel}/(d_{\perp}^{*}\omega_{\perp})=4.7\pm2$. An analysis of the integrated intensity of the two components of the EELS spectra [Fig. 1(a)], after correcting for the kinematical prefactor, and of the dipole rule gives a constant $R_0=2.5\pm0.8$. Also with such an analysis, the constant mode lifetimes are $1/\tau_{\parallel}=0.55\pm0.04$ eV and $1/\tau_{\perp}=0.33\pm0.04$ eV. Obviously, in these latter values the homogeneous and inhomogeneous (i.e., size-shape distribution) broadenings come into play. These values are in reasonable agreement with the calculated ones: $R_0=3$, $1/\tau_{\parallel}=0.34$ eV, and $1/\tau_{\perp}=0.27$ eV.

In the Ag/Si (Ref. 12) or Ag/C (Ref. 11) cases, the lack of dispersion below a critical cutoff $k_{\parallel}^{c}$ was interpreted as a signature of the confinement of the plasmon oscillation in the island. Above $k_{\parallel}^{c}$, which is inversely proportional to the mean island size, the observed frequency blue shift[12] with $k_{\parallel}$ is linked to the well-known spillout of *s* electrons in silver and reduced $s-d$ coupling at the surface.[7,23,52,54] However, for Ag/MgO, the island radius $R=1.2$ nm corresponds to a cutoff wave vector $k_{\parallel}^{c}=2\pi/2R=2.6$ nm^{-1} greater than the experimentally probed range of the reciprocal space $k_{\parallel}<1.6$ nm^{-1}, thus excluding the appearance of such a quantum blue-shift effect. Contrary to Ag/Si,[12] a dispersion is observed in conditions where the film is in the form of three-dimensional clusters, well below the percolation threshold and in the absence of substrate contributions. The appearance of two components in the plasmon peak and the observed dispersion can only be ascribed to the oscillatorlike island polarization process. However, one can argue that the quasistatic approximation used to derived the EELS cross section, Eq. (3.17), and to compute the cluster polarizability breaks down well below $k_{\parallel}^{c}$. Besides this, the herein developed model is able to describe qualitatively all the features. The computation of EELS spectra in the case of $k_{\parallel}d^{*}>1$ for supported particles would imply the knowledge of the potential everywhere in space for an approaching electron. Some attempts have been made in this direction,[55] thus including the inhomogeneities of the excitating field around the particle.

V. CONCLUSION

The cross section for electron-energy-losses was derived when the dielectric effective thickness of the surface layer, d^{*}, is smaller than the probed depth: $k_{\parallel}d^{*}\ll1$. This dielectric model is a generalization of the thin-plate model which relies on singular fields at the surface. By using the notion of surface susceptibilities, it is shown that for island layers, the cross section is driven by the particle polarizabilities as for optical excitations. The model was applied to the case of silver on silicon and MgO. Either the particle shape or the dipole selection rule explain the appearance of only one plasmon peak in most experimental studies. However, it was experimentally demonstrated for Ag/MgO that the two components of the plasmon excitation of the particles are present and that the peak dispersion versus the parallel momentum transfer is a signature of oscillatorlike polarization process of the islands. This model, which bridges the gap between optical and EELS spectra, is shown to be able to reproduce the main experimental features.

ACKNOWLEDGMENTS

We acknowledge Fabrice Didier (Saint-Gobain, France) for providing unpublished experimental results, Etienne Barthel (Laboratoire Mixte CNRS/Saint-Gobain, France) for fruitful discussions on electron-energy-loss spectroscopy, and Dick Bedeaux and Jan Vlieger (Leiden Institute of Chemistry, the Netherlands) for the preprint version of their book.[30]

APPENDIX: SURFACE MODES

The determinant of the linear system, Eq. (3.9), up to first order in $k_\parallel\gamma$ and $k_\parallel\beta$ is

$$\mathrm{Det}=\epsilon_1+\epsilon_2+k_\parallel(\gamma-\epsilon_1\epsilon_2\beta). \tag{A1}$$

In the case of a perfectly flat interface between media 1 and 2, the determinant is equal to zero when the condition $\epsilon_1+\epsilon_2=0$ for the existence of surface-plasmon waves in the nonretarded limit is fulfilled. The condition $\mathrm{Det}=0$, Eq. (A1), leads to a generalization of the dispersion relation for self-sustained surface waves in the case of a layer defined by its surface susceptibilities γ,β. Of course, the existence of these interface localized and nonradiative waves is linked to a sufficient lifetime, thus to a small damping. For a thin, metallic, continuous layer of thickness d with a Drude dielectric constant $\epsilon_c=\epsilon_a-\omega_p^2/\omega^2$ on a substrate with a frequency independent dielectric constant, the expression of the surface susceptibilities, Eqs. (3.19), leads to first order in $k_\parallel d$ to two dispersion relations

$$\omega_-=\frac{\omega_p}{\sqrt{\epsilon_a}}\left[1-\frac{1}{2}\frac{\epsilon_2}{\epsilon_a(\epsilon_1+\epsilon_2)}k_\parallel d\right],\quad \omega_+=\omega_p\sqrt{\frac{k_\parallel d}{\epsilon_1+\epsilon_2}}. \tag{A2}$$

These are the limits found from the calculation of the pole of the layer loss function[8,29,35] [(Eq. 4.2)]. The first branch of dispersion tends towards the plasmon frequency renormalized by the interband dielectric constant ϵ_a, whereas the other one towards zero for small $k_\parallel$. For small-damping oscillating dipole behavior, as it is found when a spectral representation of the islands polarizabilities is developed,[26,27,53] the surface susceptibilities read

$$\gamma=\frac{\omega_\parallel d_\parallel^*}{\omega_\parallel-\omega-i/\tau_\parallel},\quad \beta=\frac{\omega_\perp d_\perp^*}{\omega_\perp-\omega-i/\tau_\perp}. \tag{A3}$$

$d_\parallel^*, d_\perp^*$ have the dimensions of thickness and are proportional the effective oscillator strengths of the polarizability:[26] $d_\parallel=\rho/\epsilon_0 F_\parallel$, $d_\perp=\rho/(\epsilon_1^2\epsilon_0)F_\perp$. $\tau_\parallel,\tau_\perp$ define the oscillator damping. Excluding the case $\epsilon_1+\epsilon_2=0$, two dispersion relations are found at first order in $k_\parallel d_\parallel^*$, $k_\parallel d_\perp^*$:

$$\mathrm{Re}(\omega_+)=\omega_\parallel\left\{1+k_\parallel d_\parallel^*\left[\mathrm{Re}\left(\frac{1}{\epsilon_1+\epsilon_2}\right)+\frac{1}{\omega_\parallel\tau_\parallel}\mathrm{Im}\left(\frac{1}{\epsilon_1+\epsilon_2}\right)\right]\right\},$$

$$-\mathrm{Im}(\omega_+)=\frac{1}{\tau_\parallel}\left\{1-k_\parallel d_\parallel^*\omega_\parallel\tau_\parallel\mathrm{Im}\left(\frac{1}{\epsilon_1+\epsilon_2}\right)\right\},$$

$$\mathrm{Re}(\omega_-)=\omega_\perp\left\{1-k_\parallel d_\perp^*\left[\mathrm{Re}\left(\frac{\epsilon_1\epsilon_2}{\epsilon_1+\epsilon_2}\right)+\omega_\perp\tau_\perp\mathrm{Im}\left(\frac{\epsilon_1\epsilon_2}{\epsilon_1+\epsilon_2}\right)\right]\right\},$$

$$-\mathrm{Im}(\omega_-)=\frac{1}{\tau_\perp}\left\{1+k_\perp d_\perp^*\omega_\perp\tau_\perp\mathrm{Im}\left(\frac{\epsilon_1\epsilon_2}{\epsilon_1+\epsilon_2}\right)\right\}. \tag{A4}$$

It is worth noting that both types of modes are completely decoupled. At $k_\parallel=0$, the eigenmodes of the surface susceptibilities $\omega_+=\omega_\parallel,\omega_-=\omega_\perp$ are obviously recovered. For a nonabsorbing substrate, a linear dependence in $k_\parallel$ for the eigenfrequencies is observed (positive slope for the parallel mode and negative for the perpendicular mode) as well as a $k_\parallel$-constant lifetime $1/\mathrm{Im}(\omega_\pm)=\tau_{\parallel,\perp}$. Absorption in the substrate leads to a linear mode broadening with $k_\parallel$ and to a more complex behavior for the eigenfrequencies all the more than ϵ_2 depends on ω. If the layer is isolated in vacuum: $\epsilon_1=\epsilon_2=1$, the modes can be classified accordingly to their z symmetry: the ω_+ one is symmetric ($A_1=B_2$) and the ω_- one is antisymmetric ($A_1=-B_2$ with $\boldsymbol{\mathcal{D}}_S=\boldsymbol{\mathcal{E}}_S=\mathbf{0}$).

*Corresponding author. Electronic address: Lazzari@gps.jussieu.fr

†Electronic address: Jupille@gps.jussieu.fr

‡Electronic address: Layet@up.univ-mrs.fr

[1] K.D. Tsuei and E.W. Plummer, Phys. Rev. Lett. **63**, 2256 (1989).

[2] S. Suto, K.D. Tsuei, E.W. Plummer, and E. Burstein, Phys. Rev. Lett. **63**, 2590 (1989).

[3] K.D. Tsuei, E.W. Plummer, A. Liebsch, K. Kempa, and P. Bakshi, Phys. Rev. Lett. **64**, 44 (1990).

[4] M. Rocca and U. Valbusa, Phys. Rev. Lett. **64**, 2398 (1990).

[5] M. Rocca, F. Moresco, and U. Valbusa, Phys. Rev. B **45**, 1399 (1992).

[6] L. Yibing, A.C. Levi, and M. Rocca, Surf. Sci. **336**, 371 (1995).

[7] M. Rocca, Surf. Sci. Rep. **22**, 1 (1995).

[8] J.M. Layet, R. Contini, J. Derrien, and H. Lüth, Surf. Sci. **168**, 142 (1986).

[9] U. Kreibig and M. Vollmer, *Optical Properties of Metal Clusters* (Springer-Verlag, Berlin, Germany, 1995), Vol. 25.

[10] Y. Borensztein and D. Andrè, Phys. Rev. B **33**, 2828 (1986); Y. Borensztein, R. Alameh, and M. Roy, *ibid.* **50**, 1973 (1994); Y. Borensztein, M. Roy, and R. Alameh, Europhys. Lett. **31**, 311 (1995).

[11] C.M. Grimaud, L. Šiller, M. Anderson, and R.E. Palmer, Phys. Rev. B **59**, 9874 (1999).

[12] F. Moresco, M. Rocca, T. Hildebrabdt, and M. Henzler, Phys. Rev. Lett. **83**, 2238 (1999).

[13] F. Stietz and F. Träger, Philos. Mag. B **79**, 1281 (1999).

[14] F. Moresco, M. Rocca, T. Hildebrandt, and M. Henzler, Surf. Sci. **463**, 22 (2000).

[15] F. Didier, Ph.D. thesis, Université Paris XI, France, 1994.

[16] R. Lazzari, J. Jupille, and Y. Borensztein, Appl. Surf. Sci. **142**, 451 (1999).

[17] I. Simonsen, R. Lazzari, J. Jupille, and S. Roux, Phys. Rev. B **61**, 7722 (2000).

[18] M. Liehr, P. Thiry, J.J. Pireaux, and R. Caudano, Phys. Rev. B **33**, 5682 (1986).

[19] V. Coustet and J. Jupille, Surf. Sci. **307-309**, 1657 (1994); Nuovo

Cimento Soc. Ital. Fis. **19D**, 1657 (1994).
[20] M. Vermeersch, Ph.D. thesis, Faculté Universitaire, Notre-Dame de la Paix, Belgique, 1993.
[21] O. Robach, G. Renaud, and A. Barbier, Phys. Rev. B **60**, 5858 (1999).
[22] A. Barbier, G. Renaud, and J. Jupille, Surf. Sci. **454-456**, 979 (2000).
[23] J. Tiggesbäumker, L. Köller, H. Meiwes Broer, and A. Liebsch, Phys. Rev. A **48**, R1749 (1993).
[24] R. Lazzari, I. Simonsen, D. Bedeaux, J. Vlieger, and J. Jupille, Eur. Phys. J. B **24**, 267 (2001).
[25] R. Lazzari and I. Simonsen, Thin Solid Films **419**, 124 (2002).
[26] R. Lazzari, S. Roux, I. Simonsen, J. Jupille, B. Bedeaux, and V. Vlieger, Phys. Rev. B **65**, 235424 (2002).
[27] R. Lazzari, I. Simonsen, and J. Jupille, Europhys. Lett. **61**, 541 (2003).
[28] R. Lazzari, Ph.D. thesis, Université Paris XI, France, 2000.
[29] H. Ibach and D.L. Mills, *Electron Energy Loss Spectroscopy and Surface Vibrations* (Academic, New York, 1982).
[30] D. Bedeaux and J. Vlieger, *Optical Properties of Surfaces* (Imperial College Press, London, 2001).
[31] D. Bedeaux and J. Vlieger, Physica A **67**, 55 (1973); Physica (Amsterdam) **73**, 287 (1973); Physica A **82**, 221 (1976).
[32] A.M. Albano, D. Bedeaux, and J. Vlieger, Physica A **99**, 293 (1979); A.M. Albano, D. Bedeaux, and J. Vlieger, *ibid.* **102**, 105 (1980); M.T. Haarmans and D. Bedeaux, Thin Solid Films **258**, 213 (1995).
[33] J. Vlieger and D. Bedeaux, Thin Solid Films **69**, 107 (1980).
[34] D. Bedeaux and J. Vlieger, Thin Solid Films **102**, 265 (1983).
[35] H. Lüth, *Surface and Interfaces of Solids*, *Surface Science*, Vol. 15 (Springer-Verlag, Berlin, 1992).
[36] P. Lambin, J.P. Vigneron, and A.A. Lucas, Phys. Rev. B **32**, 8203 (1985).
[37] M.M. Wind and J. Vlieger, Physica A **141**, 33 (1987); *ibid.* **143**, 164 (1987); M.T. Haarmans and D. Bedeaux, Thin Solid Films **224**, 117 (1993).
[38] M.M. Wind and J. Vlieger, Physica A **125**, 75 (1984).
[39] J.D. Jackson, *Classical Electrodynamics* (Wiley, New York, 1975).
[40] L. Landau and E. Lifchitz, *Electrodynamics of Continuous Media* (Mir, Moscow, 1967).
[41] H. Ibach, Surf. Sci. **66**, 56 (1977).
[42] J.D.E. McIntyre and D.E. Aspnes, Surf. Sci. **24**, 417 (1971).
[43] R. Lazzari and I. Simonsen, GranFilm can be downloaded with a user guide from http://www.phys.ntnu.no/~ingves/Software/GranularFilm/(2001).
[44] E.D. Palik, *Handbook of Optical Constants of Solids* (Academic, New York, 1985), Vol. 1-2.
[45] T.C. Campbell, Surf. Sci. Rep. **27**, 1 (1997).
[46] C. Henry, Surf. Sci. Rep. **31**, 231 (1998).
[47] T. Yamaguchi, S. Yoshida, and A. Kinbara, Thin Solid Films **18**, 63 (1973); **21**, 173 (1974).
[48] S. Tosch and H. Neddermeyer, Phys. Rev. Lett. **61**, 349 (1988).
[49] G. Meyer and K.H. Riedier, Appl. Phys. Lett. **64**, 3560 (1994).
[50] L. Gavioli, K.R. Kimberlin, C. Tringides, J.F. Wendelken, and Z. Zhang, Phys. Rev. Lett. **82**, 129 (1999).
[51] H. Froitzheim, H. Ibach, and D.L. Mills, Phys. Rev. B **11**, 4980 (1975).
[52] A. Liebsch, Phys. Rev. B **48**, 11 317 (1993).
[53] C.E. Román-Velázquez, C. Noguez, and R.G. Barrera, Phys. Rev. B **61**, 10 427 (2000).
[54] A. Liebsch, Phys. Rev. Lett. **71**, 145 (1993).
[55] Z.L. Wang and J.M. Cowley, Ultramicroscopy **21**, 77 (1987); **21**, 335 (1987); **23**, 97 (1987); **21**, 347 (1987).